Ceramics International 45 (2019) 14873–14879

Contents lists available at ScienceDirect

Ceramics International

journal homepage: www.elsevier.com/locate/ceramint

Liquid-phase sintered bismuth ferrite multiferroics and their giant dielectric constant

N.A. Liedienov[a,b], A.V. Pashchenko[a,b,c,d,*], V.A. Turchenko[e], V.Ya. Sycheva[f], A.V. Voznyak[c], V.P. Kladko[g], A.I. Gudimenko[g], D.D. Tatarchuk[h], Y.V. Didenko[h], I.V. Fesych[i], I.I. Makoed[j], A.T. Kozakov[k], G.G. Levchenko[a,b,**]

[a] State Key Laboratory of Superhard Materials, International Centre of Future Science of Jilin University, 130012 Changchun, China
[b] Donetsk Institute for Physics and Engineering Named After O. O. Galkin, NASU, 03028 Kyiv, Ukraine
[c] Donetsk National University of Economy and Trade Named After Michael Tugan-Baranovsky, MESU, 50005 Kryvyi Rih, Ukraine
[d] Institute of Magnetism NASU and MESU, 03142 Kyiv, Ukraine
[e] Joint Institute for Nuclear Researches, 141980 Dubna, Russia
[f] Donetsk Institute for Physics and Engineering Named After O. O. Galkin, Donetsk, Ukraine
[g] V.E. Lashkaryov Institute of Semiconductor Physics, NASU, 03028 Kyiv, Ukraine
[h] National Technical University of Ukraine "Igor Sikorsky KPI", 03056 Kyiv, Ukraine
[i] Taras Shevchenko National University of Kyiv, 01030 Kyiv, Ukraine
[j] A. S. Pushkin Brest State University, 224016 Brest, Belarus
[k] Scientific-Research Institute of Physics at Southern Federal University, 344194 Rostov-na-Donu, Russia

ARTICLE INFO

Keywords:
Giant dielectric constant
Multiferroics
Perovskite structure
Defect structure
Rapid liquid-phase sintering method
XPS spectroscopy

ABSTRACT

Rapid liquid-phase sintering method has been modified and used to synthesize $Bi_{1-x}La_xFeO_{3-\delta}$ compositions ($0 \le x \le 0.5$). The temperature and sintering procedures to obtain stable single-phase samples have been defined. This provides a significant reduction in the synthesis time, which is especially important for mass production. Furthermore, giant dielectric constants have been observed in $Bi_{1-x}La_xFeO_{3-\delta}$ compositions, the values of which are one order of magnitude larger than those of similar Bi-based multiferroics obtained by conventional methods. It potentially makes them one of the most promising materials for modern technological applications.

1. Introduction

Multiferroics refer to multifunctional materials in which two or more types of ferroic ordering such as ferroelectric, ferromagnetic, and ferroelastic coexist. These materials can be used in information and energy-saving technologies to create magnetic sensors, capacitive electromagnets, magnetic memory elements, ultra-high-frequency filters, and other microelectronic and spintronic devices [1–5].

Creating film coatings with controlled properties [6] is of a particular interest and can be accomplished using both electric and magnetic fields. Effective control of the electric field can be realized only at high polarizability of the material, which led us to study its dielectric properties to determine the dielectric constant in a wide range of frequencies.

Multiferroics on the basis of bismuth ferrite ($BiFeO_3$) are multifunctional materials. Difficulty obtaining single-phase $BiFeO_3$ is related to the features of the phase diagram of the Bi_2O_3—Fe_2O_3 system [4]. In the stable equilibrium state, the main phase of $BiFeO_3$ and two impurity phases of $Bi_{25}FeO_{40}$ and $Bi_2Fe_4O_9$ oxides coexist. The preparation of single-phase $BiFeO_3$ is complicated by the volatility of bismuth above the melting point of Bi_2O_3 (817 °C) and the thermodynamic instability of $BiFeO_3$ in air is because Bi_2O_3—Fe_2O_3 solution is not in an equilibrium state [7]. Many studies have shown that the production of single-phase multiferroics using the solid state reaction method is very difficult and can be solved only within a narrow range of temperatures, compositions, and oxygen pressures [8,9].

To date, there are several ways to obtain single-phase multiferroics based on bismuth ferrite [9–12]. One is the modified Pechini method for preparing single-phase $Bi_{1-x}La_xFeO_3$ compositions with concentration of x from 0 to 0.2 [13]. Depending on the pressure (P), when the samples are pressed, significant changes in the dielectric constant (ε') and dielectric loss tangent ($\tan\delta$) occur in the low-frequency range

* Corresponding author. State Key Laboratory of Superhard Materials, International Centre of Future Science of Jilin University, 130012 Changchun, China.
** Corresponding author. State Key Laboratory of Superhard Materials, International Centre of Future Science of Jilin University, 130012 Changchun, China.
E-mail addresses: alpash@ukr.net (A.V. Pashchenko), g-levch@ukr.net (G.G. Levchenko).

https://doi.org/10.1016/j.ceramint.2019.04.220
Received 26 March 2019; Received in revised form 28 April 2019; Accepted 28 April 2019
Available online 29 April 2019

$f = 10^3$–10^7 Hz. For $Bi_{0.9}La_{0.1}FeO_3$ composition, an increase in P from 20 to 250 MPa leads to a decrease in ε' from $\sim 10^4$ to 90 and $\tan\delta$ from ~ 1 to 10^{-2} at 1 kHz. The modified Pechini method has some drawbacks related to the complexity and duration of the preparation of ceramic samples as well as the availability of a small amount of the $Bi_2Fe_4O_7$ second phase in $Bi_{1-x}La_xFeO_3$ multiferroics with concentration of $x \leq 0.05$.

As previously reported [14], rapid heating of the initial Bi_2O_3 and Fe_2O_3 oxides above 770 °C prevents the formation of $Bi_2Fe_4O_9$ and $Bi_{25}FeO_{40}$ s phases, and rapid cooling prevents the decomposition of $BiFeO_3$. Wang et al. [15] prepared ceramic $BiFeO_3$ samples using a rapid liquid-phase sintering (RLS) method and reported that the optimal temperature for obtaining single-phase $BiFeO_3$ multiferroics was 880°C for 450 s. At other sintering temperatures, the final product contained an impurity phase, which was also observed in Ref. [16]. According to dielectric spectroscopy data [16], a single-phase $BiFeO_3$ sample has low values of $\varepsilon' \sim 50$ and $\tan\delta \sim 0.1$ at 1 kHz at room temperature.

The functional properties of $BiFeO_3$ multiferroics strongly depend on the deviation from the stoichiometry of the composition and defects in the anion sublattice [17]. Investigation of structural defects, that is, the concentration of cation $V^{(c)}$ and anion $V^{(a)}$ vacancies [18] and their influence on the formation and changes in the structural, magnetic, dielectric, and ferroelectric properties of multiferroics is of particular interest [10,13,15,16,18–20]. Depending on the composition, structural defects, and method of preparing single-phase ceramic samples, it is possible to obtain materials with specified functional parameters.

We previously obtained $Bi_{1-x}La_xFeO_3$ multiferroics using the RLS method [18] at a synthesis temperature of 880 °C for 480 s. In the series of samples, 100% reproducibility of the final product was not observed because the samples obtained were partially melted after synthesis. Therefore, improving this method to determine the optimal temperature and time regimens as well as for the stable production of well-sintered ceramics is of particular interest. We are not presently aware of the cases using this method to obtain single-phase $Bi_{1-x}La_xFeO_3$ multiferroics via the isovalent replacement of Bi^{3+} by La^{3+} ions in a wide range of concentrations $x = 0$–0.5, although a reliable method is necessary for the synthesis of homogeneous $Bi_{1-x}La_xFeO_3$ samples due to their application prospects.

In the present work, we modified the RLS method to obtain single-phase $Bi_{1-x}La_xFeO_3$ multiferroics with high dielectric constant and good reproducibility of high-quality samples. The structure, defectiveness, valence state of the ions, and dielectric properties of the synthesized multifunctional $Bi_{1-x}La_xFeO_3$ materials are investigated in a wide range of concentrations and frequencies. Additionally, we conducted a careful comparative analysis of the currently available experimental results to determine the prospects for their practical application.

2. Experimental section

Ceramic $Bi_{1-x}La_xFeO_3$ samples with concentrations $x = 0$, 0.1, 0.3, and 0.5 were prepared for the first time using the modified RLS method [21]. We determined the optimal synthesis conditions, including the pressure for compacting precursors (P), temperature of synthesis (t_{synth}), synthesis time, selection of heating and cooling modes, to obtain single-phase $Bi_{1-x}La_xFeO_3$ ceramics with high reproducibility of their physical and chemical properties. High-purity La_2O_3 (≥99.5%), Bi_2O_3 (≥99.5%), and Fe_2O_3 (≥99.5%) powders were calcined at 180°C for 4 h. The obtained mixture in a stoichiometric ratio was mechanically ground in an agate mortar for 3.5 h, then compressed into tablets (Ø = 8 mm, h = 3 mm) under pressure $P = 200$ MPa and sintered at temperatures t_{synth} = 830, 840, 850, and 880°C for 450–480 s in air. The samples were sintered in a rapid heating mode at a rate of 100 °C/s from room temperature to 770 °C and at a rate of 10 °C/min from 770 °C to t_{synth}. After sintering, the samples were rapidly cooled to room temperature at a rate of 10 °C/s. The optimal conditions for well reproduced and synthesized ceramic $Bi_{1-x}La_xFeO_3$ samples are t_{synth} = 850°C for 480 s. In all of the other cases, the samples were poorly synthesized (for $t_{synth} < 850$°C) or melted (for $t_{synth} > 850$°C) and were not single-phase samples.

The type of symmetry, lattice parameters, and phase composition of the $Bi_{1-x}La_xFeO_3$ multiferroics ($x = 0$–0.5) were measured using a PANalitical X'Pert PRO MRD diffractometer in $CuK_{\alpha 1}$ radiation. The diffraction reflection patterns were recorded in the 2theta-omega mode (scanning pitch of 0.02°, time at 2 s). Qualitative phase analysis was performed using the ICDD database, PDF-2 Release 2012, and the Crystallographica Search-Match program Version 3, 1, 0, 0. Concentrations of the present phases were evaluated using the corundum numbers method [22].

The structural defects of the vacancy type and oxygen content $O_{3-\delta}$ were determined via a comparative analysis of the X-ray diffraction, thermogravimetric and iodometric titration experimental data, and previously established defect formation mechanisms for ABO_3 perovskites [18,23–26].

The microstructures and chemical compositions of the $Bi_{1-x}La_xFeO_3$ ($x = 0$–0.5) samples were studied by scanning electron microscopy (SEM) method and energy-dispersive X-ray spectroscopy (EDS) using JSM-6490-LV electron microscope.

X-ray photoelectron spectra of the ceramics and the initial Fe_2O_3, Bi_2O_3, and La_2O_3 oxide powders were obtained at room temperature with an ESCALAB 250 X-ray photoelectron microprobe. The spectra were excited with monochromatized radiation of AlK_α. The samples' surfaces were cleaned with a diamond scribing file in a vacuum in a sample preparation chamber at a pressure of approximately 10^{-6} Pa. The state of the surfaces was monitored with a C1s line. Its intensity was very small; however, the line was still detectable in the background, which allowed it to be used to calibrate the energy scales for all of the spectra. The C1s line binding energy was 285 eV. The flow of slow electrons was used to counteract the charging of the samples. The absolute energy resolution was 0.6 eV as determined from the $Ag3d_{5/2}$ line profile. Fine layers of the Fe_2O_3, Bi_2O_3, and La_2O_3 powders were deposited on double-sided conductive adhesive tape. The flow of slow electrons was also used to counteract the charging of the powders. The background of the X-ray photoelectronic lines was cut off using the Shirley method [27].

The frequency dependences of relative dielectric constant $\varepsilon'(f)$ and loss tangent $\tan\delta(f)$ were measured via dielectric spectroscopy [28] within low-frequency (LF) $f = 1$–10^6 Hz and ultra-high-frequency (UHF) $f = 8.15$–12.05 GHz ranges at room temperature. After determining the $\varepsilon'(f)$ and $\tan\delta(f)$ dependences in the LF range, cylindrical samples with a diameter of 8 mm and a height of 1 mm were used. To eliminate the possible influence of the contact resistance on the dielectric constant ε', the samples were prepared using two types of contacts. In the first case, graphite powder was applied and rubbed into the sample homogeneously over the entire surface on both sides. In the second case, the sample surface was covered with silver foil 0.1 mm thick. The $\varepsilon'(f)$ and $\tan\delta(f)$ dependences in both cases coincided within the experimental error. In further studies of the dielectric properties in the LF range, graphite powder was used to prepare the contacts.

3. Results and discussion

3.1. Structural properties of $Bi_{1-x}La_xFeO_{3-\delta}$ ceramics

X-ray diffraction patterns of the $Bi_{1-x}La_xFeO_3$ ceramics with $x = 0$, 0.1, 0.3, and 0.5 (Fig. 1) show that the main matrix structure of $BiFeO_3$ is a rhombohedral $R3m$ perovskite structure (Table 1). The composition with $x = 0$ had two additional phases of $Bi_2Fe_4O_9$ (< 2 vol.%) with an orthorhombic $Pbam$ structure ($a = 7.965$ Å, $b = 8.44$ Å, $c = 5.994$ Å, and ICCD No. 55) and $Bi_{25}FeO_{40}$ (< 2 vol.%) with a sillenite structure (cubic $I23$ structure, $a = 10.1812$ Å, and ICCD No. 197). The experimental values of the lattice parameters were listed in the hexagonal and

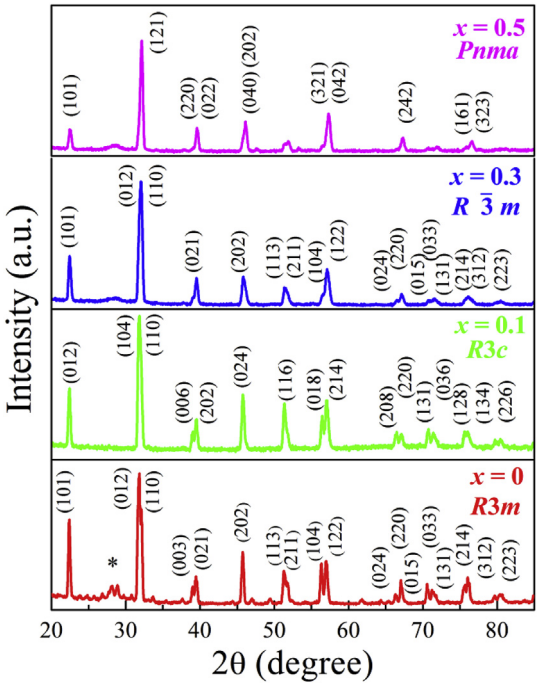

Fig. 1. X-ray diffraction patterns of the $Bi_{1-x}La_xFeO_3$ ceramics with $x = 0$, 0.1, 0.3, and 0.5. * shows the position of the diffraction peak from the $Bi_2Fe_4O_9$ and $Bi_{25}FeO_{40}$ oxides.

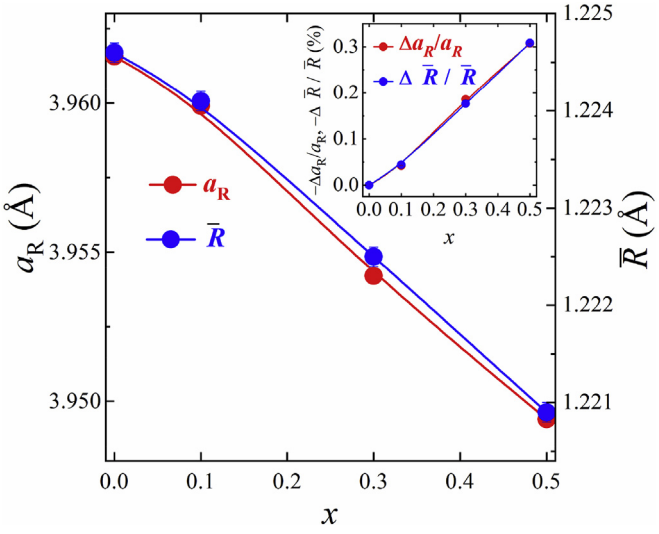

Fig. 2. Concentration changes in the lattice parameter a_R and average ionic radius $\bar{R}$ for the perovskite $Bi_{1-x}La_xFeO_{3-\delta}$ structure. The inset shows the correlation of the relative changes in the parameter $\Delta a_R/a_R$ and the average ionic radius $\Delta\bar{R}/\bar{R}$ (the error in determining the structural parameters corresponds to the size of the experimental point markers).

rhombohedral installations (Table 1). In Fig. 1, the absence of diffraction maxima from the Bi_2O_3, Fe_2O_3, and La_2O_3 oxides made it possible to conclude the complete polymorphic transformation of the initial oxides with the formation of a perovskite $Bi_{1-x}La_xFeO_3$ structure. The availability of the $Bi_2Fe_4O_9$ and $Bi_{25}FeO_{40}$ oxides is observed only in non-doped $BiFeO_3$ within a range of $2\theta = 27.5–29.0^\circ$ angles (* in Fig. 1). The appearance of a halo in this range of angles for compositions with $x = 0.3$ and 0.5 indicates the initiation of $Bi_2Fe_4O_9$ and $Bi_{25}FeO_{40}$ in the form of amorphous-like microinclusions. All of the measured X-ray patterns were obtained within the resolution of the PANalitical X'Pert PRO MRD diffractometer over the range of $2\theta = 20–90^\circ$ angles at increments of 0.025°, which provides the accuracy of the lattice parameter determination with an accuracy of 0.0001 Å and rhombohedral angle α_R with an accuracy 0.005°. This leads to the conclusion that the $Bi_{1-x}La_xFeO_3$ samples are single-phase with $x = 0.1–0.5$ and have a negligible amount of second phase for the non-doped $BiFeO_3$.

The sillenite phase in bismuth ferrite may have a chemical composition of $Bi_{25}FeO_{40}$ with Bi^{3+} and Bi^{5+} or $Bi_{25}FeO_{39}$ only with Bi^{3+}. If one bismuth ion in a unit cell has an oxidation state of +5, the chemical formula is $Bi^{3+}_{24}[Bi^{5+}Fe^{3+}]O^{2-}_{40}$ [29]. In the sillenite structure of $Bi_{25}FeO_{40}$, the Bi^{3+} ions occupy the octahedral positions, forming a cage of corner-connected polyhedrons, whereas the Bi^{5+} and Fe^{3+} ions share the tetrahedral positions within the cage [30]. According to the X-ray data (see Supplementary Material, Fig. 1S), the XRD patterns of $Bi_{25}FeO_{40}$ and $Bi_{25}FeO_{39}$ are identical. Since the XRD study can not accurately determine the chemical composition of the sillenite phase, the more general formula $Bi_{25}FeO_{40}$ for the $Bi_{1-x}La_xFeO_3$ sample with $x = 0$ (see Table 1) was used.

The rhombohedral structure of the $Bi_{1-x}La_xFeO_3$ samples in course of the replacement of Bi^{3+} by La^{3+} ions undergoes a series of distortions from *R*3*m* for $x = 0$ to *R*3*c* for $x = 0.1$ and *R*$\bar{3}$*m* for $x = 0.3$ and becomes orthorhombic *P*nma for $x = 0.5$ (Table 1). The transition from the space group *R*3*m* for $x = 0$ to *R*3*c* for $x = 0.1$ is associated with the appearance of the rotations of oxygen octahedron FeO_6 along the [111] direction in the ferroelectric phase relative to the structure of an ideal cubic perovskite [31]. The change in the spatial group from *R*3*c* to *R*$\bar{3}$*m* with increasing x from 0.1 to 0.3 indicates a decrease in the tilt distortion in the polar rhombohedral $Bi_{0.7}La_{0.3}FeO_3$ structure. The appearance of the non-polar *P*nma orthorhombic *O** phase [32] in the composition with $x = 0.5$ is due to the rotation of the octahedral FeO_6 complexes along the [110] direction [33].

As shown in Fig. 2, the lattice parameter a_R correlates with the average ionic $\bar{R}$ radius of the perovskite structure [23] and decreases with the increase in the concentration x. Such changes in the structural properties in course of an isovalent substitution of Bi^{3+} ($R = 1.50$ Å) cations by La^{3+} ions ($R = 1.50$ Å) with identical ionic radii R [34,35] are caused by decreasing $V^{(a)}$ concentration [36]. According to the principle of electroneutrality, an increase in the charge of the anion sublattice with a decrease in the concentration of $V^{(a)}$ vacancies from 5.7 to 3.3% is compensated by a decrease in the concentration of Fe^{2+} from 0.32 to 0.18% and an increase in the concentration of Fe^{3+} from

Table 1
Phase composition, structure type, and lattice parameters of the $Bi_{1-x}La_xFeO_3$ ceramics obtained using the modified RLS method.

x	Type	Space group	ICDD No.	Lattice parameters					Second phase (vol. %)	
				hexagonal			rhombohedral			
				a (Å)	b (Å)	c (Å)	a_R (Å)	α_R (°)	$Bi_{25}FeO_{40}$	$Bi_2Fe_4O_9$
0	rhombohedral	*R*3*m*	160	5.5737	–	6.9339	3.9616	89.52	< 2	< 2
0.1	rhombohedral	*R*3*c*	161	5.5730	–	13.8480	3.9599	89.51	–	–
0.3	rhombohedral	*R*$\bar{3}$*m*	166	5.5694	–	6.8927	3.9589	89.53	–	–
0.5	orthorhombic	*P*nma	62	5.5771	7.8650	5.5486	3.9494	89.52	–	–

Table 2
The molar formulas of the defect perovskite structure, concentration of anion $V^{(a)}$ vacancies, and tolerance factor t in the $Bi_{1-x}La_xFeO_{3-\delta}$ ceramics.

x	Molar formulas of defect perovskite structure	$V^{(a)}$ (%)	t
0	$\{Bi^{3+}_{0.99}V^{(c)}_{0.01}\}_A[Fe^{2+}_{0.32}Fe^{3+}_{0.68}]O^{2-}_{2.83}V^{(a)}_{0.17}$	5.7	0.940
0.1	$\{Bi^{3+}_{0.89}La^{3+}_{0.10}V^{(c)}_{0.01}\}_A[Fe^{2+}_{0.30}Fe^{3+}_{0.70}]_BO^{2-}_{2.84}V^{(a)}_{0.16}$	5.3	0.941
0.3	$\{Bi^{3+}_{0.69}La^{3+}_{0.30}V^{(c)}_{0.01}\}_A[Fe^{2+}_{0.24}Fe^{3+}_{0.76}]_BO^{2-}_{2.87}V^{(a)}_{0.13}$	4.3	0.945
0.5	$\{Bi^{3+}_{0.49}La^{3+}_{0.50}V^{(c)}_{0.01}\}_A[Fe^{2+}_{0.18}Fe^{3+}_{0.82}]_BO^{2-}_{2.90}V^{(a)}_{0.10}$	3.3	0.948

0.68 to 0.82% in the cation sublattice (Table 2). The appearance of Fe^{3+} ions in *B*-positions with a smaller ionic radius $R = 0.785$ Å instead of Fe^{2+} with a large ionic radius $R = 0.92$ Å [35] explains the decrease in the lattice parameter (Fig. 2 and Table 1).

Vacancy type structural defects (cation $V^{(c)}$ and anion $V^{(a)}$ vacancies) strongly influence the valence state of cations, lengths of the metal-oxygen bonds, coordination numbers, and inhomogeneity of the nearest environment, causing a change in the stability of the perovskite structure and its structural properties. As shown in Refs. [37,38], only vacancy type point defects (Schottky defects) can exist in the close-packed perovskite structure without the formation of interstitial point defects (Frenkel defects).

Based on the comparative X-ray analysis and thermogravimetric and iodometric titration data (see Supplementary material) using the defect formation model [23,24], the molar formulas of a real perovskite $Bi_{1-x}La_xFeO_{3-\delta}$ structure were determined and are listed in Table 2. In rare-earth perovskites, the average valence of 3*d* metal in a state of variable valence depends on the oxygen index, that is, on the concentration of $V^{(a)}$, and can be determined from the iodometric titration data [26] (see Table 1S). The concentration of $V^{(a)}$ correlates with the thermogravimetric analysis data (see Fig. 2S) since with increasing La concentration from $x = 0$ to 0.5, the decrease in the mass loss of samples $\Delta m/m$ after their synthesis from -3.295 to -1.487% is due to a decrease in $V^{(a)}$ from 5.7 to 3.3% (see Table 2 and Fig. 2S).

The validity of the molar formulas determined for the defect $Bi_{1-x}La_xFeO_{3-\delta}$ structure (see Table 2) is confirmed by Fig. 2, which shows that the relative changes in the average ionic radius $\Delta\bar{R}/\bar{R}$ coincide quite accurately with the relative changes in the lattice parameter of the unit cell $\Delta a_R/a_R$ according to the correlations between $\Delta\bar{R}/\bar{R}$ and $\Delta a_R/a_R$ for a perovskite structure previously established [24,26]. Fig. 2 is a generalized result of the established correlation between the X-ray diffraction and thermogravimetric and iodometric titration data since the average radius $\bar{R}$ depends on the valence of the ions, the oxygen content, and the concentration of the $V^{(c)}$ and $V^{(a)}$ vacancies [24,25].

The real structure of the $Bi_{1-x}La_xFeO_{3-\delta}$ contains *A* cations of Bi^{3+}_A and La^{3+}_A, *B* cations of Fe^{2+}_B and Fe^{3+}_B, O^{2-} anions, and anion $V^{(a)}$ and cation $V^{(c)}$ vacancies. The appearance of cation $V^{(c)}$ vacancies ~ 1 at.% in the *A* sublattice in all of the compounds (Table 2) is due to the volatility of bismuth when samples are sintered (850 °C) above the melting point (817 °C) of bismuth Bi_2O_3 oxide. According to EDS data, the chemical composition of the $Bi_{1-x}La_xFeO_3$ approximately agrees with nominal composition 1:1:3. The measured atomic percentages of Bi, La, and Fe are 19.32%, 0%, and 20.47% for $x = 0$, 17.20%, 2.28%, and 20.89% for $x = 0.1$, 12.64%, 6.77%, and 19.96% for $x = 0.3$, and 9.49%, 10.51%, and 19.97% for $x = 0.5$, respectively, also confirming non-stoichiometry in the *A* sublattice of all of the compositions.

Table 2 shows the relationship between the concentration of the anion $V^{(a)}$ vacancies and the tolerance factor $t = (R_A + R_X)/(\sqrt{2}(R_B + R_X))$ [39]. The tolerance factor for the ideal cubic perovskite is $t = 1$ and its structure consists of close-packed octahedral FeO_6 complexes around a BiO_{12} cuboctahedron [14,23]. The increase in the tolerance factor *t* with the decrease in the concentration of the $V^{(a)}$ vacancies (Table 2) is caused by a decrease in the average radius of the *B* cations as a result of the $Fe^{2+}_B \rightarrow Fe^{3+}_B$ transition. Increasing the average valence of the *B* cations leads to a decrease in the radius of the *A* position, an increase in the tolerance factor *t*, and an increase in the stability of the perovskite structure $t \rightarrow 1$. The deviation of the *A* position radius from the average *A* cation $\bar{R}_A$ radius of the perovskite $Bi_{1-x}La_xFeO_{3-\delta}$ structure leads to tilt distortions, which increases its stability due to the close-packed octahedral FeO_6 complexes around the BiO_{12} polyhedron.

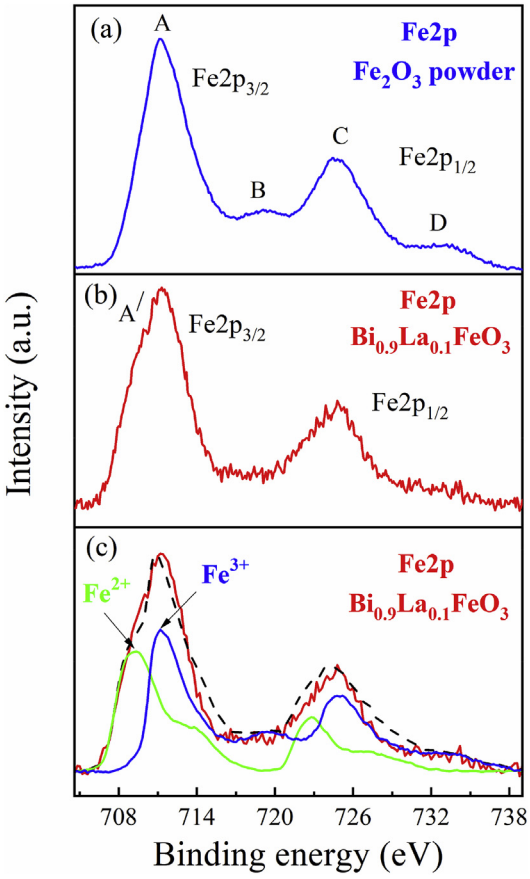

Fig. 3. X-ray photoelectron spectra of Fe2p of the Fe_2O_3 powder (a), $Bi_{0.9}La_{0.1}FeO_3$ ceramics (b), and its decomposition into components (c) related to the Fe2p spectrum from Fe^{2+} ions (green curve) and Fe^{3+} (blue curve). (For interpretation of the references to colour in this figure legend, the reader is referred to the Web version of this article.)

Additionally, to assess the real $Bi_{1-x}La_xFeO_{3-\delta}$ structure, XPS spectroscopy investigations were conducted on the $Bi_{0.9}La_{0.1}FeO_3$ composition. Fig. 3 shows a comparative analysis of the X-ray photoelectron spectra of the initial Fe_2O_3 powder and $Bi_{0.9}La_{0.1}FeO_3$ sample. As demonstrated in Fig. 3 (a), the Fe2p spectrum consists of two maxima A and C at a distance of 23.6 eV related to the $Fe2p_{3/2}$ and $Fe2p_{1/2}$ levels, respectively. In addition to these main features of the spectra, at a distance of 7.8 eV from the maximum of A, there is a singularity B (719 eV) and after the peak C, there is a diffuse shelf D (733 eV). The features of C and D refer to satellites of charge transfer. Moreover, the availability of singularity C and the value of binding energy equal to 711.2 eV indicate that the iron ions in the sample are in the trivalent state [40–42].

The spectrum in Fig. 3 (b) has an energy A/lower than the maximum of A at a distance of approximately 1.8 eV. In addition, there is no feature B in the spectrum. These differences from the Fe2p spectrum in Fig. 3 (a) indicate that the spectrum of the Fe_3O_4 sample has Fe^{2+} and Fe^{3+} ions [41].

To clarify the availability of the different valence iron ions in the ceramic $Bi_{0.9}La_{0.1}FeO_3$ sample, the experimental spectrum was decomposed (Fig. 3 (c)) using the approach in Ref. [40] in components related to bivalent and trivalent iron ions. As shown in Fig. 3c, the Fe2p

spectrum of the ceramic sample is described quite well by the sum of the components related to Fe^{2+} and Fe^{3+} with proportions of 26% and 74%, respectively. While estimating the contributions, it was taken into account that the ionization probability of the 2p shell in the Fe^{2+} ion is two times higher in the Fe^{3+} ion [40].

Trivalent state of Bi^{3+} and La^{3+} ions in corresponding Bi_2O_3, La_2O_3 powders and $Bi_{0.9}La_{0.1}FeO_3$ composition was confirmed by XPS spectroscopy (see Figs. 3S and 4S, Supplementary Material).

3.2. Dielectric properties of $Bi_{1-x}La_xFeO_{3-\delta}$ multiferroics

The main goal of synthesizing bismuth perovskites is to obtain multiferroics with dielectric properties useful for various applications. Therefore, the investigation of the dielectric properties of $Bi_{1-x}La_xFeO_{3-\delta}$ multiferroics is important for determining the possibility and area of their application. To the best of our knowledge, the dielectric constant is usually measured at a frequency above 1 kHz. Our measurements were carried out starting from 1 Hz. This makes it possible to obtain the real dielectric constant in a DC field. At room temperature, the dielectric constant ε' in the $BiFeO_3$ multiferroic depends on the frequency and varies from $\varepsilon' \sim 10^4$ in the LF (f = 1 Hz–1 MHz) [43] to $\varepsilon' \sim 12$ in the UHF (f = 8–12 GHz) [44] ranges. Unexpectedly, giant dielectric constant occurred for all of the samples. Fig. 4 shows that the dielectric constant ε' and dielectric loss tangent $\tan\delta = \varepsilon''/\varepsilon'$ have a relaxation type of dispersion and at room temperature all of the compositions have anomalously high values of $\varepsilon' = 10^5$–$5{\cdot}10^5$ at 1 Hz. These values decrease non-monotonically to $\varepsilon' \sim 106$–209 with increase in the frequency to f = 1 MHz. The $Bi_{1-x}La_xFeO_{3-\delta}$ sample with x = 0.1 has the highest values of $\varepsilon' = 5{\cdot}10^5$ (at 1 Hz) and 209 (at 1 MHz).

In ionic oxide polycrystals within the LF range, the main mechanisms of dielectric polarization include: (i) electron hopping between the same crystallographic positions occupied by ions of the same type but with different valences and (ii) intergranular polarization associated with the migration and accumulation of weakly coupled carriers on structural inhomogeneities, grain boundaries, and structural defects [45,46]. The most likely reason for the appearance of giant dielectric constant in the LF range is a result of polarization caused by both the numerous structural defects and the high conductivity in the $Bi_{1-x}La_xFeO_{3-\delta}$ samples. In structural defects, polarization arises when quasi-free charges accumulate at the crystallite boundaries or are localized near vacancy type point defects, which leads to the polarization of the material and increases the real dielectric constant ε'. An additional increase in ε' is also due to the conductivity. For large losses $\tan\delta \sim 1$ (see Fig. 4) related to the conductivity, the samples can be presented not as insulators with large losses, but as conductors with a significant imaginary component of the electrical conductivity σ''. The availability of the imaginary component σ'' is equivalent to adding the quantity σ''/ω [47] to the dielectric constant ε'. The shift σ'' in phase by $\pi/2$ relative to the applied voltage is associated with the delay and accumulation of quasi-free charge carriers on structural inhomogeneities and structural defects.

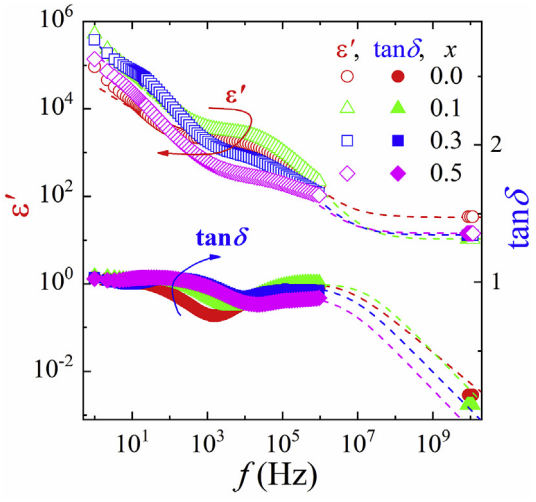

Fig. 4. The frequency dependences of the dielectric constant $\varepsilon'(f)$ and dielectric loss tangent $\tan\delta(f)$ of the $Bi_{1-x}La_xFeO_{3-\delta}$ ceramics. The labels show the experimental data for ε' and $\tan\delta$; the dashed lines indicate their approximation.

In the UHF range f = 8–12 GHz, the ε_∞ and $\tan\delta$ become frequency-independent for all of the compositions. With increase in the La^{3+} content, an increase in ε_∞ from 10.7 (x = 0.10) to 14.5 (x = 0.50) and a decrease in $\tan\delta$ from $3{\cdot}10^{-3}$ (x = 0.10) to $1{\cdot}10^{-4}$ (x = 0.50) are observed. For bismuth ferrite (x = 0), the values of ε_∞ and $\tan\delta$ are equal to 34.5 and $2{\cdot}10^{-3}$, respectively. Such high values of ε_∞ for $BiFeO_3$ are possibly associated with the influence of the second impurity phase.

The frequency dependence of the $\varepsilon^* = \varepsilon' + i\varepsilon''$ components, which are in good agreement with the experimental data, can be described by the following relationships [48–50]:

$$\varepsilon' = \varepsilon_\infty + \frac{(\varepsilon_s - \varepsilon_\infty)[1+(\omega\tau)^{1-\alpha}\sin(\pi\alpha/2)]}{1 + 2(\omega\tau)^{1-\alpha}\sin(\pi\alpha/2)+(\omega\tau)^{2(1-\alpha)}} + \frac{(\varepsilon_{s1} - \varepsilon_{\infty1})[1 + (\omega\tau_2)^{\gamma}\sin(\pi\gamma/2)]}{1 + 2(\omega\tau_2)\sin(\pi\gamma/2) + (\omega\tau_2)^{2\gamma}} + \frac{\sigma_1}{\varepsilon_0\omega^{\beta_1}}, \quad (1)$$

$$\varepsilon'' = \frac{(\varepsilon_s - \varepsilon_\infty)(\omega\tau)^{1-\alpha}\cos(\pi\alpha/2)}{1 + 2(\omega\tau)^{1-\alpha}\sin(\pi\alpha/2)+(\omega\tau)^{2(1-\alpha)}} + \frac{(\varepsilon_{s1} - \varepsilon_{\infty1})(\omega\tau_2)^{\gamma}\cos(\pi\gamma/2)}{1 + 2(\omega\tau_2)\sin(\pi\gamma/2) + (\omega\tau_2)^{2\gamma}} + \frac{\sigma_2}{\varepsilon_0\omega^{\beta_2}}, \quad (2)$$

where ε_s is a static dielectric constant, and ε_∞ is a high-frequency dielectric constant. The parameters α, γ, and β characterize the distributions of the relaxation times τ determined in the first approximation from the condition $\omega_{max}{\cdot}\tau = 1$, where ω_{max} is the frequency corresponding to the maximum of $\tan\delta$. The second and third terms in Eq. (1) are mathematical expressions describing the Debye model in different frequency intervals with the Cole-Cole and Cole-Davidson distributions of the relaxation times [48,49], respectively.

On the basis of the simulation, the $\varepsilon'(f)$ and $\tan\delta(f)$ spectra can be represented as the result of the coexistence of various mechanisms of dielectric polarization and their contributions to the dielectric constant (Figs. 5–9S, Supplementary Material). At high frequencies, the contribution to the dielectric constant is due to electron, ion, and ferroelectric (movement of domain walls or ferroelectric domains) polarizations. Their resulting contribution is described by the ε_∞ term in the high-frequency limit. The origin of the dielectric relaxation can be explained by oscillations of the ferroelectric domain walls. The domain walls vibrate in an alternating electric field and are effective converters of transverse waves. Wave radiation has a maximum when the length of the sound wave is comparable to the width of the domain. Above this frequency, the domain walls can no longer vibrate due to inertia and do not contribute to the dielectric constant. Based on the simulation results (see Supplementary Material), this contribution exists in a range up to 10^8 Hz. As the frequency decreases, the polarization mechanism caused by electron hopping between different valence $Fe^{2+} \leftrightarrow Fe^{3+}$ cations present in a frequency range up to $\sim 10^6$ Hz. The contribution to the resulting dielectric constant from the LF mechanisms prevails starting from 280 Hz and up to the static limit.

The second term in Eq. (1) can be related to the electron hopping mechanism between the $Fe^{2+} \leftrightarrow Fe^{3+}$ ions, which is in the frequency range from 10^3 to 10^6 Hz [51,52]. It is confirmed by decreasing the maxima of $\tan\delta$ from 1.08 (x = 0.10) to 0.47 (x = 0.50) within a frequency range 10^3–10^6 Hz, which well correlates with the decrease in the concentration of the Fe^{2+} ions as a result of a decrease in the concentration of the $V^{(a)}$ vacancies (Table 2).

The third term in Eq. (1) describes the high-frequency relaxation

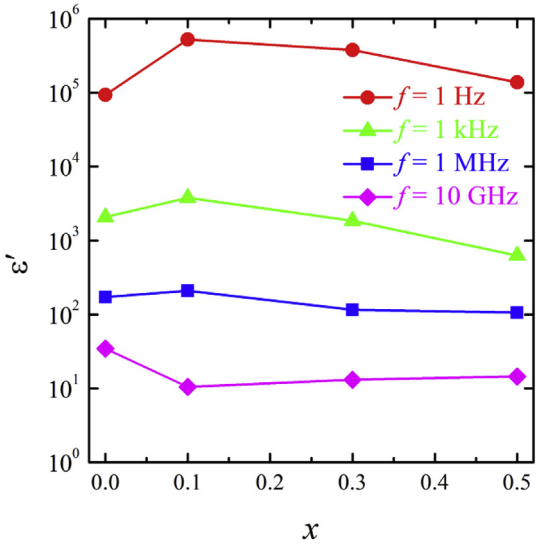

Fig. 5. The concentration dependences of dielectric constant ε′ for the $Bi_{1-x}La_xFeO_{3-\delta}$.

mechanism of the dielectric polarization, the nature of which has not been finally clarified. A possible mechanism of the dielectric polarization in a frequency range from 10^7 to 10^9 Hz is the motion of the walls of the ferroelectric domains [52,53].

The appearance of ferroelectric properties in the non-polar *Pnma* phase requires additional analysis of the XRD data for the $Bi_{1-x}La_xFeO_3$ ceramics with $x = 0.5$. The appearance of the second non-centrosymmetric $Pn2_1a$ structure [54] is observed in the rare earth *Ln* modified $Bi_{1-x}Ln_xFeO_3$ at the transition of the polar *R*3*c* to the non-polar *Pnma* phase. Rietveld refinement of the XRD patterns for both of these *Pnma* and $Pn2_1a$ space groups give practically identical reliability factors. To accurately determine the type of *Pnma* or $Pn2_1a$ structure, additional studies of the ferroelectric and magnetic properties [55] should be conducted. An analysis of the dielectric properties for the $Bi_{1-x}La_xFeO_3$ ceramics with $x = 0.5$ in the UHF range leads to the conclusion that the motion of the ferroelectric walls in $Bi_{0.5}La_{0.5}FeO_3$ is a result of the coexistence of the polar $Pn2_1a$ and non-polar *Pnma* structures.

In the LF limit, which is described by the last term in Eqs. (1) and (2), the large values of tanδ are due to the contributions of quasi-free carriers of the electric current to the dielectric polarization, that is, dielectric losses are related to the conductivity and accumulation of electric charge on the intercrystalline boundaries, inhomogeneities, and structural defects within a framework of the Maxwell-Wagner and Kups models [56,57]. The decreasing crystallite sizes were confirmed by SEM data with an increase in concentration of the La^{3+} ions from $x = 0$ to 0.1 (see Fig. 10S, Supplementary Material). This leads to the sharp increase in the intergranular area and causes the increase in the ε′ at $f = 1$ Hz with an increase in x from 0 to 0.1 (red curve, Fig. 5). As the frequency increases from 1 Hz to 1 MHz, the influence of the boundaries on the resistivity between the crystallites decreases and the increase in the ε′ becomes smaller at higher frequencies (green and blue curves, Fig. 5). The reduction in the ε′ at $f = 10$ GHz (pink curve, Fig. 5) is not due to the accumulation of the carriers on the intercrystalline boundaries, but because of the motion of the ferroelectric domain walls. With the increase in the x, at frequencies up to 1 MHz, the decrease in the concentration of Fe^{2+} ions and $V^{(a)}$ vacancies plays a decisive role in the ε′ change. However, at frequencies of 1 MHz and 10 GHz, their influence also decreases and ε′ does not depend on the concentration of La^{3+}, Fe^{2+}, and $V^{(a)}$.

Eqs. (1) and (2) make it possible to obtain model spectra the parameters of which are given in Table 3. The parameters characterize the dispersion of ε′ in different frequency ranges and can be used as characteristics required for application. The deviation between the theoretical calculations and the experimental data does not exceed the error of the experiment within the frequency interval.

4. Conclusions

Ceramic $Bi_{1-x}La_xFeO_{3-\delta}$ samples with $x = 0$–0.5 were prepared via the modified rapid liquid-phase sintering method. It was established that at sintering temperatures of 830, 840, 850, and 880°C (for 450–480 s), $t_{synth} = 850$°C for 480 s is optimal for obtaining single-phase $Bi_{1-x}La_xFeO_{3-\delta}$ ceramics with anomalously high values of the dielectric constant within the LF range at room temperature.

It has been established that the transition from a rhombohedral to an orthorhombic perovskite structure and the decrease in the lattice parameters in the $Bi_{1-x}La_xFeO_{3-\delta}$ ceramics in the course of isovalent replacement of Bi^{3+} ($R = 1.50$ Å) by La^{3+} ($R = 1.50$ Å) are not only because of the change in the average ionic radius of the *B* cation as a result of the change in the Fe^{3+}/Fe^{2+} ratio, but are also due to the change in the concentration of vacancy type point defects.

The molar formulas of the real defect perovskite $Bi_{1-x}La_xFeO_{3-\delta}$ structure were determined. The real structure contains *A* cations of Bi_A^{3+} and La_A^{3+}, *B* cations of different valences of Fe_B^{2+} and Fe_B^{3+} ions, and O^{2-} anions as well as anion $V^{(a)}$ and cation $V^{(c)}$ vacancies.

All of the compositions at room temperature have giant dielectric constant ε′ greater than 10^5 at 1 Hz. According to the Maxwell-Wagner polarization model, anomalously high values of ε′ are due to the accumulation of charges at the grain boundaries, inhomogeneities, and structural defects. The optimal $Bi_{0.9}La_{0.1}FeO_{3-\delta}$ composition with the highest dielectric constant $\varepsilon' = 5{\cdot}10^5$ at 1 Hz was determined. These promising materials with giant dielectric constant can be used for modern technological applications.

Acknowledgements

This work was partially supported by The Thousand Talents Program for Foreign Experts program of China (project WQ20162200339), the Ministry of Education and Science of Ukraine (award No. 16BF037-01), the Ministry of Education and Science of the Russian Federation (award No. 3.6105.2017/8.9) and the State Scientific Research Program 2016-2020, Physical materials science, new materials and technology (subprogram Material Science and Technology of Materials, task No. 1.35).

Appendix A. Supplementary data

Supplementary data to this article can be found online at https://doi.org/10.1016/j.ceramint.2019.04.220.

Table 3
The dielectric parameters (τ, α, ε_s, ε_∞, σ_1, β_1, σ_2, β_2, τ_2, γ, ε_{s1}, and $\varepsilon_{\infty 1}$) of model spectra for the $Bi_{1-x}La_xFeO_{3-\delta}$ ceramics obtained using the modified RLS method.

x	τ (10^{-5} s)	α	ε_s	ε_∞	σ_1 ($10^{-7}\,\Omega^{-1}\,m^{-1}$)	β_1	σ_2 ($10^{-7}\,\Omega^{-1}\,m^{-1}$)	β_2	τ_2 (10^{-5} s)	γ	ε_{s1}	$\varepsilon_{\infty 1}$
0	3.98	0.135	500	33.65	2.90	0.597	2.95	0.597	1.98	0.955	1898	500
0.1	3.92	0.050	2100	10.65	29.99	0.898	32.99	0.770	1.26	0.987	3700	2100
0.3	2.58	0.040	600	13.22	30.42	0.810	32.00	0.784	0.58	0.940	990	600
0.5	1.01	0.040	110	14.46	17.90	0.890	25.61	0.890	0.25	0.899	370	110

References

[1] M. Opel, Spintronic oxides grown by laser-MBE, J. Phys. D Appl. Phys. 45 (2012) 033001.
[2] A.P. Pyatakov, A.K. Zvezdin, Magnetoelectric and multiferroic media, Phys. Usp. 55 (2012) 557–581.
[3] Z. Kutnjak, J. Petzelt, R. Blinc, The giant electromechanical response in ferroelectric relaxors as a critical phenomenon, Nature 441 (2006) 956–959.
[4] A. Maitre, M. François, J.C. Gachon, Experimental study of the Bi_2O_3–Fe_2O_3 pseudo-binary system, J. Phase Equilibria Diffusion 25 (2004) 59–67.
[5] M. Etier, V.V. Shvartsman, S. Salamon, Y. Gao, H. Wende, D.C. Lupascu, The direct and the converse magnetoelectric effect in multiferroic cobalt ferrite–barium titanate ceramic composites, J. Am. Ceram. Soc. 99 (2016) 3623–3631.
[6] J. Ma, J. Hu, Z. Li, C.W. Nan, Recent progress in multiferroic magnetoelectric composites: from bulk to thin films, Adv. Mater. 23 (2011) 1062–1087.
[7] M.S. Bernardo, T. Jardiel, M. Peiteado, A.C. Caballero, M. Villegas, Reaction pathways in the solid state synthesis of multiferroic $BiFeO_3$, J. Eur. Ceram. Soc. 31 (2011) 3047–3053.
[8] M. Thrall, R. Freer, C. Martin, F. Azough, B. Patterson, R.J. Cernik, An in situ study of the formation of multiferroic bismuth ferrite using high resolution synchrotron X-ray powder diffraction, J. Eur. Ceram. Soc. 28 (2008) 2567–2572.
[9] P. Suresh, S. Srinath, A comparative study of sol-gel and solid-state prepared La^{3+} doped multiferroic $BiFeO_3$, Adv. Mater. Lett. 5 (2014) 127–130.
[10] Q. Zhang, X. Zhu, Y. Xu, H. Gao, Y. Xiao, D. Liang, J. Zhu, J. Zhu, D. Xiao, Effect of La^{3+} substitution on the phase transitions, microstructure and electrical properties of $Bi_{1-x}La_xFeO_3$ ceramics, J. Alloy. Comp. 546 (2013) 57–62.
[11] M. Popa, D. Crespo, J.M. Calderon-Moreno, S. Preda, V. Fruth, Synthesis and structural characterization of single-phase $BiFeO_3$ powders from a polymeric precursor, J. Am. Ceram. Soc. 90 (2007) 2723–2727.
[12] E. Mostafavi, A. Ataie, M. Ahmadzadeh, Characterization of nano-structured multiferroic bismuth ferrite produced via solid state reaction route, Adv. Mater. Res. 829 (2014) 683–687.
[13] Q.-H. Jiang, C.-W. Nan, Z.-J. Shen, Synthesis and properties of multiferroic La-modified $BiFeO_3$ ceramics, J. Am. Ceram. Soc. 89 (2006) 2123–2127.
[14] S.M. Selbach, Mari-Ann Einarsrud, T. Grande, On the thermodynamic stability of $BiFeO_3$, Chem. Mater. 21 (2009) 169–173.
[15] Y.P. Wang, L. Zhou, M.F. Zhang, X.Y. Chen, J.-M. Liu, Z.G. Liu, Room-temperature saturated ferroelectric polarization in $BiFeO_3$ ceramics synthesized by rapid liquid phase sintering, Appl. Phys. Lett. 84 (2004) 1731–1733.
[16] A.K. Pradhan, K. Zhang, D. Hunter, J.B. Dadson, G.B. Loiutts, P. Bhattacharya, R. Katiyar, J. Zhang, D.J. Sellmyer, U.N. Roy, Y. Cui, A. Burger, Magnetic and electrical properties of single-phase multiferroic $BiFeO_3$, J. Appl. Phys. 97 (2005) 093903.
[17] L.R. Dedon, S. Saremi, Z. Chen, A.R. Damodaran, B.A. Apgar, R. Gao, L.W. Martin, Nonstoichiometry, structure, and properties of $BiFeO_3$ films, Chem. Mater. 28 (2016) 5952–5961.
[18] A.V. Pashchenko, D.D. Tatarchuk, N.A. Liedienov, V.V. Burchovetski, V.K. Prokopenko, V.Ya Sycheva, N.E. Pismenova, Y.V. Didenko, G.G. Levchenko, Structure imperfection and dielectric properties of single-phase multifferoic $Bi_{1-x}La_xFeO_{3-\delta}$, 2016, IEEE 36th International Conference on Electronics and Nanotechnology (ELNANO) (2016) 107–109.
[19] I.O. Troyanchuk, D.V. Karpinsky, M.V. Bushinsky, V.A. Khomchenko, G.N. Kakazei, J.P. Araujo, M. Tovar, V. Sikolenko, V. Efimov, A.L. Kholkin, Isothermal structural transitions, magnetization and large piezoelectric response in $Bi_{1-x}La_xFeO_3$ perovskites, Phys. Rev. B 83 (2011) 054109.
[20] H. Chou, C.-W. Yen, C.-C. Yang, G.D. Dwivedi, K.S. Yang, C.P. Wu, K.C. Liu, W.-H. Li, Oxygen deficiency-induced anomalous enhancement of Neel temperature and magnetic coupling for $Bi_{0.9}Ca_{0.1}FeO_{3-\delta}$ and $Bi_{0.9}Pb_{0.1}FeO_{3-\delta}$, Acta Mater. 111 (2016) 297–304.
[21] O.V. Pashchenko, D.D. Tatarchuk, M.O. Liedienov, Y.V. Didenko, V.K. Prokopenko, Y.M. Poplavko, Method for Obtaining Single-phase Multiphoerics on the Basis of Bismuth Ferrite, (2018) UA patent 126094.
[22] C.R. Hubbard, R.L. Snyder, RIR - measurement and use in quantitative XRD, Powder Diffr. 3 (1988) 74–77.
[23] A.V. Pashchenko, V.P. Pashchenko, V.K. Prokopenko, YuF. Revenko, YuS. Prylipko, N.A. Ledenev, G.G. Levchenko, V.P. Dyakonov, H. Szymczak, Influence of structure defects on functional properties of magnetoresistance $(Nd_{0.7}Sr_{0.3})_{1-x}Mn_{1+x}O_3$ ceramics, Acta Mater. 70 (2014) 218–227.
[24] A.V. Pashchenko, V.P. Pashchenko, V.K. Prokopenko, V.A. Turchenko, YuF. Revenko, A.S. Mazur, V.Ya Sycheva, N.A. Liedienov, V.G. Pitsyuga, G.G. Levchenko, Role of structure imperfection in the formation of the magneto-transport properties of rare-earth manganites with a perovskite structure, J. Exp. Theor. Phys. 124 (2017) 100–113.
[25] A.V. Pashchenko, V.P. Pashchenko, N.A. Liedienov, V.K. Prokopenko, YuF. Revenko, N.E. Pismenova, V.V. Burhovetskii, V.Y. Sycheva, A.V. Voznyak, G.G. Levchenko, V.P. Dyakonov, H. Szymczak, Structure, phase transitions, ^{55}Mn NMR, magnetic and magnetotransport properties of the magnetoresistance $La_{0.9-x}Ag_xMn_{1.1}O_{3-\delta}$ ceramics, J. Alloy. Comp. 709 (2017) 779–788.
[26] A.V. Pashchenko, N.A. Liedienov, V.P. Pashchenko, V.K. Prokopenko, V.V. Burhovetskii, A.V. Voznyak, I.V. Fesych, D.D. Tatarchuk, Y.V. Didenko, A.I. Gudymenko, V.P. Kladko, A.A. Amirov, G.G. Levchenko, Modification of multifunctional properties of the magnetoresistive $La_{0.6}Sr_{0.15}Bi_{0.15}Mn_{1.1-x}B_xO_{3-\delta}$ ceramics when replacing manganese with 3d-ions of Cr, Fe, Co, Ni, J. Alloy. Comp. 767 (2018) 1117–1125.
[27] D. Briggs, M.P. Seach, Practical Surface Analysis, Auger and X-Ray Photoelectron Spectroscopy, John Wiley&Sons, Chichester, New York, Brisbane, Toronto, Singapore, 1984.
[28] D.D. Tatarchuk, V.I. Molchanov, V.M. Pashkov, A.S. Franchuk, Microwave Dielectric measurement methods on the base of the composite dielectric resonator, 2015, IEEE 35th International Conference on Electronics and Nanotechnology ELNANO-2015 (2015) 231–234.
[29] D.C. Craig, N.C. Stephenson, Structural studies of some body-centered cubic phases of mixed oxides involving Bi_2O_3: the structures of $Bi_{25}FeO_{40}$ and $Bi_{38}ZnO_{60}$, J. Solid State Chem. 15 (1975) 1–8.
[30] N. Rangavittal, T.N.G. Row, C.N.R. Rao, A study of cubic bismuth oxides of theType $Bi_{26-x}M_xO_{40-\delta}$ (M = Ti, Mn, Fe, Co, Ni or Pb) related to gamma-Bi_2O_3, Eur. J. Solid State Inorg. Chem. 31 (1994) 409–422.
[31] Y.K. Jeong, C.W. Bark, S. Ryu, J.-H. Lee, H.M. Jang, R3c-R3m octahedron-tilting transition in rhombohedrally-distorted $BiFeO_3$ multiferroics, J. Korean Phys. Soc. 58 (2011) 817–820.
[32] D. Kan, L. Palova, V. Anbusathaiah, C.J. Cheng, S. Fujino, V. Nagarajan, K.M. Rabe, I. Takeuchi, Universal behavior and electric-field-induced structural transition in rare-earth-substituted $BiFeO_3$, Adv. Funct. Mater. 20 (2010) 1108–1115.
[33] P. Ravindran, R. Vidya, A. Kjekshus, H. Fjellvag, Theoretical investigation of magnetoelectric behavior in $BiFeO_3$, Phys. Rev. B 74 (2006) 224412.
[34] P. Boutinaud, Revisiting the spectroscopy of the Bi^{3+} ion in oxide compounds, Inorg. Chem. 52 (2013) 6028–6038.
[35] R.D. Shannon, Revised effective ionic radii and systematic studies of interatomic distances in halides and chalcogenides, Acta Crystallogr. A 32 (1976) 751–767.
[36] A.V. Pashchenko, V.P. Pashchenko, V.K. Prokopenko, YuF. Revenko, A.S. Mazur, V.V. Burchovetskii, V.A. Turchenko, N.A. Liedienov, V.G. Pitsyuga, G.G. Levchenko, V.P. Dyakonov, H. Szymczak, The role of structural and magnetic inhomogeneities in the formation of magneto-transport properties of the $La_{0.6-x}Sm_xSr_{0.3}Mn_{1.1}O_{3-\delta}$ ceramics, J. Magn. Magn. Mater. 416 (2016) 457–465.
[37] L. Malavasi, Role of defect chemistry in the properties of perovskite manganites, J. Mater. Chem. 18 (2008) 3295–3308.
[38] R.A. De Souza, M.S. Islam, E. Ivers-Tiffee, Formation and migration of cation defects in the perovskite oxide $LaMnO_3$, J. Mater. Chem. 9 (1999) 1621–1627.
[39] F.A. Kassan-Ogly, V.E. Naish, The immanent chaotization of crystal structures and the resulting diffuse scattering. II. Crystallochemical conditions of perovskite chaotization, Acta Crystallogr. B42 (1986) 307–313.
[40] A.T. Kozakov, A.G. Kochur, K.A. Googlev, A.V. Nikolsky, I.P. Raevski, V.G. Smotrakov, V.V. Yeremkin, X-ray photoelectron study of the valence state of iron in iron-containing single-crystal ($BiFeO_3$, $PbFe_{1/2}Nb_{1/2}O_3$), and ceramic ($BaFe_{1/2}Nb_{1/2}O_3$) multiferroics, J. Electron. Spectrosc. Relat. Phenom. 184 (2011) 16–23.
[41] T. Yamashita, P. Hayes, Analysis of XPS spectra of Fe^{2+} and Fe^{3+} ions in oxide materials, J. Appl. Surf. Science 254 (2008) 2441–2449.
[42] A. Tovstolytkin Navjot, G.S. Lotey, Plasmonic enhanced photocatalytic activity of Ag nanospheres decorated $BiFeO_3$ nanoparticles, Catal. Lett. 147 (2017) 1640–1645.
[43] J. Lu, A. Gunther, F. Schrettle, F. Mayr, S. Krohns, P. Lunkenheimer, A. Pimenov, V.D. Travkin, On the room temperature multiferroic $BiFeO_3$: magnetic, dielectric and thermal properties, Eur. Phys. J. B. 75 (2010) 451–460.
[44] Y. Li, X. Fang, M. Cao, Thermal frequency shift and tunable microwave absorption in $BiFeO_3$ family, Sci. Rep. 6 (2016) 24837.
[45] J. Lu, A. Gunther, F. Schrettle, F. Mayr, S. Krohns, P. Lunkenheimer, A. Pimenov, V.D. Travkin, A.A. Mukhin, A. Loidl, On the room temperature multiferroic $BiFeO_3$: magnetic, dielectric and thermal properties, Eur. Phys. J. B. 75 (2010) 451–460.
[46] A. Singh, R. Chatterjee, S.K. Mishra, P.S.R. Krishna, S.L. Chaplot, Origin of large dielectric constant in La modified $BiFeO_3$-$PbTiO_3$, J. Appl. Phys. 111 (2012) 1–7 014113.
[47] C.-S. Tu, T.-H. Wang, V.H. Schmidt, R.R. Chien, Origin of low-frequency dielectric permittivity in $BiFeO_3$ multiferroic ceramics, IEEE Conference Publication for ISAF/PFM 2011 International Symposium on Applied of Ferroelectrics, Vancouver, BC, 2011, pp. 24–27.
[48] K.S. Cole, R.H. Cole, Dispersion and absorption in dielectrics I. Alternating current characteristics, J. Chem. Phys. 9 (1941) 341–351.
[49] D.W. Davidson, R.H. Cole, Dielectric relaxation in glycerol, propylene glycol, and nPropanol, J. Chem. Phys. 19 (1951) 1484–1490.
[50] K. Majhi, B.S. Prakash, K.B.R. Varma, Extreme values of relative permittivity and dielectric relaxation in Sr_2SbMnO_6 ceramics, J. Phys. D Appl. Phys. 40 (2007) 7128–7135.
[51] S. Habouti, C.-H. Solterbeck, M. Es-Souni, UV assisted pyrolysis of solution deposited $BiFeO_3$ multiferroic thin films. Effects on microstructure and functional properties, J. Sol. Gel Sci. Technol. 42 (2007) 257–263.
[52] Z.X. Cheng, A.H. Li, X.L. Wang, S.X. Dou, K. Ozawa, H. Kimura, S.J. Zhang, T.R. Shrout, Structure, ferroelectric properties, and magnetic properties of the La-doped bismuth ferrite, J. Appl. Phys. 103 (2008) 07E507.
[53] D.O. Alikin, A.P. Turygin, J. Walker, A. Bencan, B. Malic, T. Rojac, V.Ya Shur, A.L. Kholkin, The effect of phase assemblages, grain boundaries and domain structure on the local switching behavior of rare-earth modified bismuth ferrite ceramics, Acta Mater. 125 (2017) 265–273.
[54] V.A. Khomchenko, D.A. Kiselev, I.K. Bdikin, V.V. Shvartsman, P. Borisov, W. Kleemann, J.M. Vieira, A.L. Kholkin, Crystal structure and multiferroic properties of Gd-substituted $BiFeO_3$, Appl. Phys. Lett. 93 (2008) 262905-1 - 262905-3.
[55] W. Hu, Y. Chen, H. Yuan, G. Li, Y. Qiao, Y. Qin, S. Feng, Structure, magnetic, and ferroelectric properties of $Bi_{1-x}Gd_xFeO_3$ nanoparticles, J. Phys. Chem. C 115 (2011) 8869–8875.
[56] J. Lu, A. Günther, F. Schrettle, F. Mayr, S. Krohns, P. Lunkenheimer, A. Pimenov, V.D. Travkin, A.A. Mukhin, A. Loidl, On the room temperature multiferroic $BiFeO_3$: magnetic, dielectric and thermal properties, Eur. Phys. J. B 75 (2010) 451–460.
[57] C.G. Koops, On the dispersion of resistivity and dielectric constant of some semiconductors at audiofrequencies, Phys. Rev. 83 (1951) 121–124.